

Nonreciprocal quantum phase transition in a spinning microwave magnonic system

Ye-jun Xu,^{1,*} Long-hua Zhai,¹ Peng Fu,¹ Shou-jing Cheng,¹ and Guo-Qiang Zhang^{2,†}

¹*Interdisciplinary Research Center of Quantum and Photoelectric Information,
and Anhui Research Center of Semiconductor Industry Generic Technology, Chizhou University, Chizhou, Anhui, 247000, China*

²*School of Physics, Hangzhou Normal University, Hangzhou 311121, China*

(Dated: May 15, 2024)

We propose how to achieve nonreciprocal quantum phase transition in a spinning microwave magnonic system composed of a spinning microwave resonator coupled with an yttrium iron garnet sphere with magnon Kerr effect. Sagnac-Fizeau shift caused by the spinning of the resonator brings about a significant modification in the critical driving strengths for second- and one-order quantum phase transitions, which means that the highly controllable quantum phase can be realized by the spinning speed of the resonator. More importantly, based on the difference in the detunings of the counterclockwise and clockwise modes induced by spinning direction of the resonator, the phase transition in this system is nonreciprocal, that is, the quantum phase transition occurs when the system is driven in one direction but not the other. Our work offers an alternative path to engineer and design nonreciprocal magnonic devices.

I. INTRODUCTION

Quantum phase transition (QPT) has attracted considerable attention for its crucial role in quantum physics and potential applications in modern quantum technologies [1–16]. Different from the classical phase transition happening in a finite temperature, this type of phase transition is mainly originated from the quantum fluctuation at the critical parameter regime and can take place between two stable phases accompanied by spontaneous symmetry breaking as the temperature tends to the absolute zero of temperature. Usually, a QPT occurs in the thermodynamic limit involving a infinite number of system components. Although recent advances about QPTs have indicated that the thermodynamic limit may be no longer a requirement [17–19], the QPT observed in infinite-component system is still one of the most fascinating topics. Recently, it is interesting that that a squeezed light driving high-quality cavity can give rise to QPT in a dissipative qubit collective system without the ultra-strongly nonlinear coupling between the atoms and the field [20]. Additionally, the QPTs have also been studied in dissipative systems with other types of nonlinearity, such as the Kerr nonlinearity [21, 22]. Among them, it was confirmed that a QPT can emerge in a Kerr-nonlinear oscillator subject to two-photon driving and single-photon loss. Moreover, based on the magnon Kerr effect owing to the magnetocrystalline anisotropy in the ferromagnetic yttrium-iron-garnet sphere, the studies on QPT have made progress in hybrid cavity magnonic systems in recent years. In Ref. [23], the authors studied the parity-symmetry-breaking QPT in a single-cavity magnonic system driven by a parametric field. This system can show a rich phase diagram, including the parity-symmetric phase (PSP), parity-symmetry-broken phase (PSBP), and bistable phase (BP). Subsequently, a controllable QPT was also proposed in a double-cavity magnonic system [24]. In particular, they demonstrated that the phase transition in one cavity can be precisely and efficiently controlled

by adjusting the parameters of the other cavity. Nonetheless, whether the controllability of QPT can be realized only in a single-cavity magnonic system is still a question worth exploring.

Nonreciprocal physics, referring to the phenomenon that a system displays different responses in opposite directions, has witnessed rapid advances in recent years. Up to now, the study of nonreciprocity has been extended to many scientific branches, such as optics [25, 26], acoustics [27–29], thermodynamics [30]. As an important application, nonreciprocal devices allow signals to propagate in one direction and prevents signals from propagating in the opposite direction, and therefore plays a key role in backaction-immune communications. Traditional nonreciprocal devices break Lorentz reciprocity to achieve nonreciprocity mainly by employing the Faraday effect in magneto-optical crystal materials [31, 32], but such devices needs the magnetic materials that are bulky, costly, and unsuitable for on-chip integration due to the high susceptibility to external magnetic field interference. To circumvent these obstacles, a variety of nonreciprocity schemes have been proposed based on nonlinear optics [33–36], optomechanics [37–39], non-Hermitian optics [40–43]. Especially, a recent experiment confirmed that an optical diode with 99.6% isolation has been realized by using a spinning resonator [44], in which the nonreciprocity is caused by the Fizeau shift of circulating lights. Subsequently, there is increasing interests in the connection of the nonreciprocity with other quantum effects, such as nonreciprocal quantum blockades [45–54], quantum entanglement [55–58], mechanical squeezing [59–61], phonon and magnon laser [62–64], and sideband responses [65, 66]. Very recently, one particular concern is that nonreciprocal superradiant phase transitions have been reported in a cavity QED system [67].

Here we propose how to achieve an nonreciprocal QPT in a single spinning microwave resonator coupled to an yttrium iron garnet (YIG) sphere with magnon Kerr nonlinearity. We show that, compared with the case of double-cavity, the QPT can be efficiently controlled only by adjusting the angular speed of the resonator without introducing an auxiliary resonator. Physically, the value of the order parameter for characterizing QPT is strongly dependent on the detun-

* yejunxu@126.com

† zhangguoqiang@hznu.edu.cn

ing between the cavity field and the driving laser. Meanwhile, the Sagnac effect caused by the spinning of the resonator can result in different influences on the detuning of the counter-clockwise (CCW) and clockwise (CW) fields compared to the driving laser. Therefore, nonreciprocal QPT occurs by reason of the significant difference in the mean magnon number for driving the resonator from the opposite directions. Specifically, our system can display a rich phase diagram containing PSP, PSBP, and BP. Furthermore, we show that the system can experience a second-order phase transition from a PSP to a PSBP or a first-order phase transition from a PSP to a BP when increasing the driving strength beyond a critical value under different initial conditions. More importantly, in comparison to the stationary case, the tunable nonreciprocal QPT can be achieved by the Sagnac effect. Furthermore, we investigate the different behaviors of the mean magnon number and correlation fluctuation in the vicinity of the critical point and find that these behaviors can be used to identify different phase transitions. In addition, an isolation parameter is introduced to quantitatively describe the nonreciprocal degree. The results indicate again that the QPT can be readily switched on and off by adjusting the driving direction or the spinning direction of the resonator.

The remainder of this paper is organized as follows. In Sec. II, we introduce the theoretical model and give the dynamics and the steady-state solutions of the system through Heisenberg-Langevin approach. In Sec. III, the impact of the Sagnac-Fizeau shift and the rotating direction of the resonator on the nonreciprocal behaviors of the QPT are studied in detail. Finally, we summarize our results in Sec. IV.

II. THE MODEL

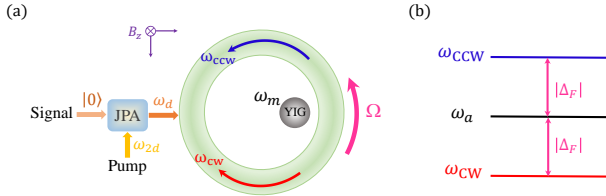


FIG. 1. (a) Schematic of the system. A YIG sphere with magnon Kerr nonlinearity is placed inside a spinning microwave resonator driven by a squeezed light generated by a flux-driven JPA and simultaneously biased by a uniform magnetic field along the z direction. (b) Frequencies of the microwave resonator. When the microwave resonator rotates in the fixed counterclockwise (CCW) direction, the resonance frequencies of the CCW mode and clockwise (CW) mode will experience different Fizeau shifts, where the frequencies $\omega_a + |\Delta_F|$ and $\omega_a - |\Delta_F|$ denote for the CCW and CW modes, respectively.

As schematically shown in Fig. 1, we consider a cavity-magnon system which is composed of a spinning microwave resonator coupled to a YIG sphere via the magnetic dipole interaction. While the resonator is driven by a weak squeezed vacuum field generated by a flux-driven Josephson parametric

amplifier (JPA) and the magnetocrystalline anisotropy results in the Kerr nonlinear interaction among magnons in the YIG sphere. The Hamiltonian of the total system reads ($\hbar = 1$)

$$H = (\omega_a + \Delta_F) a^\dagger a + \omega_m m^\dagger m + \frac{K}{2} m^\dagger m^\dagger m m + J(a^\dagger m + a m^\dagger) + \frac{G}{2} (a^{\dagger 2} e^{-2i\omega_d t} + a^2 e^{2i\omega_d t}), \quad (1)$$

where a (a^\dagger) and m (m^\dagger) are, respectively, the annihilation (creation) operators of the cavity and magnon modes with the corresponding resonance frequencies ω_a and ω_m . The microwave resonator is parametrically driven with driving amplitude G and pump frequency ω_d . K denotes the nonlinear coefficient of the magnon Kerr effect and J is the strength of the cavity-magnon interaction. For a resonator spinning at an angular velocity Ω , the frequencies of the CCW and CW modes experience Sagnac-Fizeau shift, i.e., $\omega_a \rightarrow \omega_a + \Delta_F$, with

$$\Delta_F = \pm \Omega \frac{nr\omega_a}{c} \left(1 - \frac{1}{n^2} - \frac{\lambda}{n} \frac{dn}{d\lambda} \right), \quad (2)$$

in which n is the refractive index, r is the radius of the resonator, and λ (c) is the wavelength (speed) of the light in vacuum. The dispersion term $dn/d\lambda$, characterizing the relativistic origin of the Sagnac effect, is relatively small ($\sim 1\%$) and thus can be ignored. In the rotating frame with respect to the driven frequency ω_d , the Hamiltonian of the system becomes

$$H = \tilde{\Delta}_a a^\dagger a + \Delta_m m^\dagger m + \frac{K}{2} m^\dagger m^\dagger m m + J(a^\dagger m + a m^\dagger) + \frac{G}{2} (a^{\dagger 2} + a^2), \quad (3)$$

with $\tilde{\Delta}_a = \Delta_a + \Delta_F$, $\Delta_a = \omega_a - \omega_d/2$, $\Delta_m = \omega_m - \omega_d/2$.

By considering dissipation and noise effects in the Hamiltonian (3), the quantum Langevin equations (QLEs) describing the dynamics of the hybrid system can be written as

$$\begin{aligned} \dot{a} &= -i(\tilde{\Delta}_a - i\kappa)a - iJm - iGa^\dagger + \sqrt{2\kappa}a_{in}, \\ \dot{m} &= -i(\Delta_m - i\gamma)m - iKm^\dagger m - iJa + \sqrt{2\gamma}m_{in}, \end{aligned} \quad (4)$$

where κ (γ) and a_{in} (m_{in}) are the damping rate and the zero-mean input noise operator for the cavity (magnon) mode, respectively. Furthermore, a linearization procedure can be used to simplify the physical model. We expand the operators a and m in Eq. (4) as a sum of their expectation values and small quantum fluctuations, $a = A + \delta a$ ($m = M + \delta m$). By using the mean-field approximation, it follows from Eq. (4) that the dynamical equations for the expectation values are

$$\begin{aligned} \dot{A} &= -i(\tilde{\Delta}_a - i\kappa)A - iJM - iGA^*, \\ \dot{M} &= -i(\Delta_m - i\gamma)M - iK|M|^2 M - iJA. \end{aligned} \quad (5)$$

In the steady-state case ($\dot{A} = \dot{M} = 0$), solving Eq. (5) gets three solutions for the mean magnon number $|M|^2$, i.e.,

$$|M|_0^2 = 0, \quad |M|_\pm^2 = \frac{-\tilde{\Delta}_m \pm \sqrt{\tilde{\Delta}_m^2 - \tilde{\gamma}^2}}{K}, \quad (6)$$

with $\tilde{\Delta}_m = \Delta_m - \beta\tilde{\Delta}_a$, $\tilde{\gamma} = \gamma + \beta\kappa$, $\beta = J^2 / (\tilde{\Delta}_a^2 + \kappa^2 - G^2)$. According to the first equation in Eq. (5), the steady-state photon occupation can be expressed as

$$|A|_0^2 = 0, \quad |A|_{\pm}^2 = \frac{(\tilde{\Delta}_m + |M|_{\pm}^2)^2 + \gamma^2}{g^2} |M|_{\pm}^2, \quad (7)$$

hence we need only to consider the mean magnon number $|M|^2$ as an order parameter to characterize the QPT of the system. In order to derive critical conditions of the phase transition, we first concentrate our attention on $|M|_+^2 \geq 0$. In the case of $-\tilde{\Delta}_m \geq 0$ (i.e., $\Delta_m/\tilde{\Delta}_a \leq \beta$), we take $\xi^2 G^2 - \tilde{\gamma}^2 = 0$ in Eq. (6), which gives rise to $G = G_{c1}$ with

$$G_{c1} = \frac{-g^2 + \sqrt{4\gamma^2\tilde{\Delta}_a^2 + (g^2 + 2\gamma\kappa)^2}}{2\gamma}. \quad (8)$$

Thus the critical driving strength G_{c1} is independent of the detuning Δ_m . In the other case, when $-\tilde{\Delta}_m \leq 0$ and $\sqrt{\xi^2 G^2 - \tilde{\gamma}^2} \geq 0$, the critical driving strength is

$$G_{c2} = \sqrt{\frac{(g^2 - \tilde{\Delta}_a\Delta_m)^2 + \gamma^2\tilde{\Delta}_a^2 + 2g^2\gamma\kappa + \gamma^2\kappa^2 + \Delta_m^2\kappa^2}{\gamma^2 + \Delta_m^2}}. \quad (9)$$

It clearly see from Eqs. (8) and (9) that both critical driving strengths are subject to the Fizeau shift Δ_F . Secondly, we can use the nontrivial solution $|M|_-^2$ to obtain the third phase transition point even if it is proved to be unstable in the following. By only considering the case $-\tilde{\Delta}_m \geq 0$ and $\sqrt{\xi^2 G^2 - \tilde{\gamma}^2} \geq 0$, we obtain the critical driving strength $G = G_{c2}$, which has the same form as Eq. (9).

On the other hand, the linearized QLEs for quantum fluctuations can be written as

$$\begin{aligned} \delta\dot{a} &= -i(\tilde{\Delta}_a - i\kappa)\delta a - iJ\delta m - iG\delta a^\dagger + \sqrt{2\kappa}\delta a_{in}, \\ \delta\dot{m} &= -i(\tilde{\Delta}_m - i\gamma)\delta m - iJ\delta a - iKM^2\delta m^\dagger + \sqrt{2\gamma}\delta m_{in}, \end{aligned} \quad (10)$$

with $\tilde{\Delta}_m = \Delta_m + 2K|M|^2$. Here we have neglected the high-order terms of the fluctuations and δo_{in} is the fluctuation on top of o_{in} ($o = a, m$). By defining the quadrature operators $\delta Q = (\delta a^\dagger + \delta a)/\sqrt{2}$, $\delta P = i(\delta a^\dagger - \delta a)/\sqrt{2}$, $\delta X = (\delta m^\dagger + \delta m)/\sqrt{2}$, $\delta Y = i(\delta m^\dagger - \delta m)/\sqrt{2}$, Eq. (10) can be rewritten in a compact matrix form

$$\delta\dot{\mathbf{O}} = \mathbf{U} \cdot \delta\mathbf{O} + \delta\mathbf{O}_{in}, \quad (11)$$

with the vector of quadrature components $\delta\mathbf{O} = (\delta Q, \delta P, \delta X, \delta Y)^T$ and the vector of noise quadratures $\delta\mathbf{O}_{in} = (\sqrt{2\kappa}\delta Q_{in}, \sqrt{2\kappa}\delta P_{in}, \sqrt{2\gamma}\delta X_{in}, \sqrt{2\gamma}\delta Y_{in})^T$. The superscript ‘T’ denotes the transpose. The drift matrix \mathbf{U} takes the form

$$\mathbf{U} = \begin{pmatrix} -\kappa & \Pi_+ & 0 & J \\ \Pi_- & -\kappa & -J & 0 \\ 0 & J & \Theta_+ & \Xi_+ \\ -J & 0 & \Xi_- & \Theta_- \end{pmatrix}, \quad (12)$$

with $\Pi_{\pm} = \pm\tilde{\Delta}_a - G$, $\Theta_{\pm} = -\gamma \pm K\text{Im}[M^2]$ and $\Xi_{\pm} = \pm\tilde{\Delta}_m - K\text{Re}[M^2]$. For a given solution of M in Eq. (5), only if all eigenvalues of the matrix \mathbf{U} have negative real parts, the solution is said to be stable, otherwise this solution is unstable. After numerically carrying out this stability analysis [see Fig. 2(a)-2(c) and related discussions], we find that the nontrivial solution $|M|_-^2$ is always unstable in the whole parameter space, while the solutions $|M|_-^2$ and $|M|_+^2$ are stable in some parameter space, which suggests that we only need to apply the solutions $|M|_0^2$ and $|M|_+^2$ to investigate the steady-state quantum phase transitions. In addition, to research the variances of magnon mode quadratures, we define the time-dependent covariance matrix $V(t)$ with $V_{ij}(t) = \langle f_i(t)f_j(t') + f_j(t')f_i(t) \rangle / 2$ ($i, j = 1, 2, 3, 4$). From Eq. (11), one can easily find the solutions of $V(\infty)$ by solving the so-called Lyapunov equation $\mathbf{U}\mathbf{V} + \mathbf{V}\mathbf{U}^T = -\mathbf{D}$ with \mathbf{D} being the diffusion matrix, defined as $\mathbf{D}_{ij}(t-t') = \langle \delta\mathbf{O}_{in,i}(t)\delta\mathbf{O}_{in,j}(t') + \delta\mathbf{O}_{in,j}(t')\delta\mathbf{O}_{in,i}(t) \rangle / 2$. The diagonal elements of the matrix \mathbf{V} associate with the variance of quadratures. In our model, the variance of magnon mode quadrature is given by $\langle \delta m^\dagger \delta m \rangle = [(\mathbf{V}_{33} + \mathbf{V}_{44}) - 1] / 2$.

III. NONRECIPROCAL QUANTUM PHASE TRANSITION

In this section, we explore how to realize a nonreciprocal QPT via the spinning of the resonator. We begin by employing the standard stability analysis to show the phase diagrams against the reduced driving strength G/κ and the ratio $\Delta_m/\tilde{\Delta}_a$. As illustrated in Figs. 2(a)-2(c), each steady-state phase diagram exists three different regions corresponding to different phases, i.e., PSP, PSBP, and BP. The vertical black solid line ($G = G_{c1}$) is the boundary between PSP and BP in the case of $\Delta_m/\tilde{\Delta}_a \leq \beta|_{G=G_{c1}}$, and then the blue and red solid curves ($G = G_{c2}$) are the boundaries between PSP and PSBP for $\Delta_m/\tilde{\Delta}_a \geq \beta|_{G=G_{c1}}$, BP and PSBP for $\Delta_m/\tilde{\Delta}_a \leq \beta|_{G=G_{c1}}$, respectively. These manifest that the boundaries between different phases are determined by the critical driving strengths G_{c1} and G_{c2} . In particular, the intersection point of three boundaries emerges when $G_{c1} = G_{c2}$ at $\Delta_m/\tilde{\Delta}_a = \beta|_{G=G_{c1}}$. More interestingly, we find that different spinning directions (the left or right) give rise to QPT at different critical driving strength. Compared with the stationary case (i.e., no spinning with $\Delta_F = 0$), the areas of three phases have a remarkable change for $\Delta_F > 0$ and $\Delta_F < 0$. Therefore, this QPT is highly controllable and can be tuned by the driving direction (or the spinning direction) and the spinning speed of the resonator. As a result, the nonreciprocal QPT can be achieved in this system.

In Figs. 3(a)-2(c), we further display the dynamical behaviors of the scaled mean magnon number $|M|^2 / (\gamma/K)$ to reveal the macroscopic magnon excitations for different phases. Here the parameter values for each phase have marked with different-colored dots in Fig. 2(b). When the system is in BP [see Fig. 3(a)], we find that both the solutions $|M|_0^2$ and $|M|_+^2$ are stable and the steady-state magnon occupation can be dominated by the initial condition of the system. This situa-

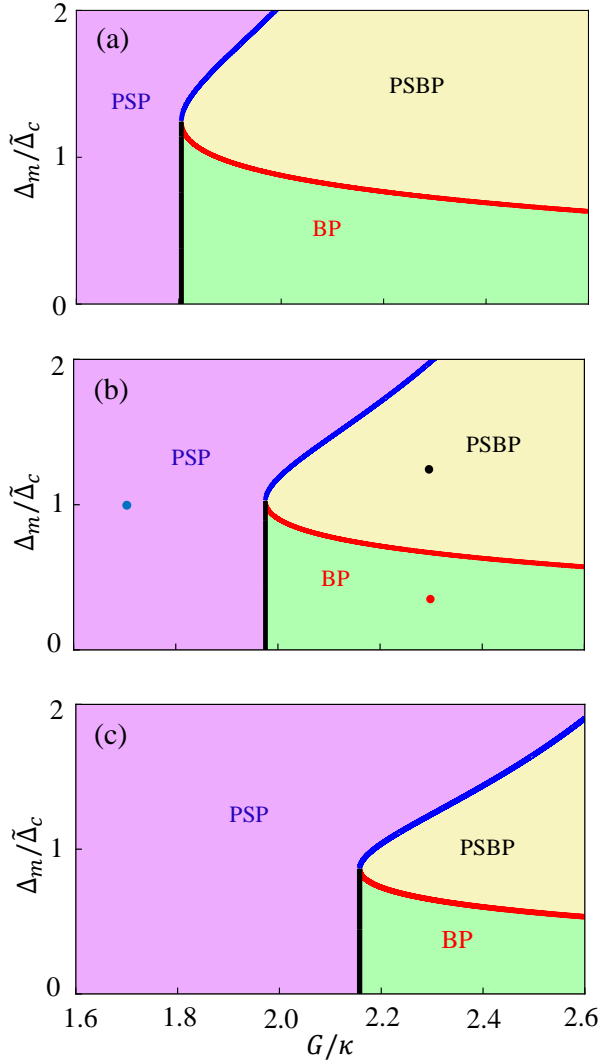


FIG. 2. Steady-state phase diagram of the system varying with the reduced driving strength G/κ and the detuning ratio Δ_m/Δ_c , in which PSP, PSBP, and BP represent the areas for the parity-symmetric phase, parity-symmetry-broken phase and bistable phase, respectively. The Fizeau shifts are $\Delta_F/\kappa = -0.3$ in (a), $\Delta_F/\kappa = 0$ in (b), and $\Delta_F/\kappa = 0.3$ in (c). The other parameters are $\Delta_c/\kappa = 3$, $J/\kappa = 2.5$, and $\gamma/\kappa = 1$.

tion indicates that the parity symmetry in BP can be conserved or broken with appropriate initial conditions. It is noticed that PSP and BP will cannot be distinguished by only tracking the dynamics of the system with an initial state near zero since the solution $|M|_0^2$ is stable for both phases. In this case, the initial state should be set far away from zero to distinguish the two phases and observe the phase transition. From Fig. 3(b), we see that only the nontrivial solution $|M|_+^2$ becomes stable in PSBP. The system has the macroscopic magnon excitation in this phase and thus is parity-symmetry broken. As described in Fig. 3(c), there is no macroscopic magnon excitation in PSP, that is to say, only the solution $|M|_0^2$ is stable and then the system is parity symmetric. Besides, an interesting feature is that the nontrivial solution $|M|_-^2$ is always unstable in

the whole parameter range since the four eigenvalues of the matrix \mathbf{U} in Eq. (12) have at least one nonnegative real part.

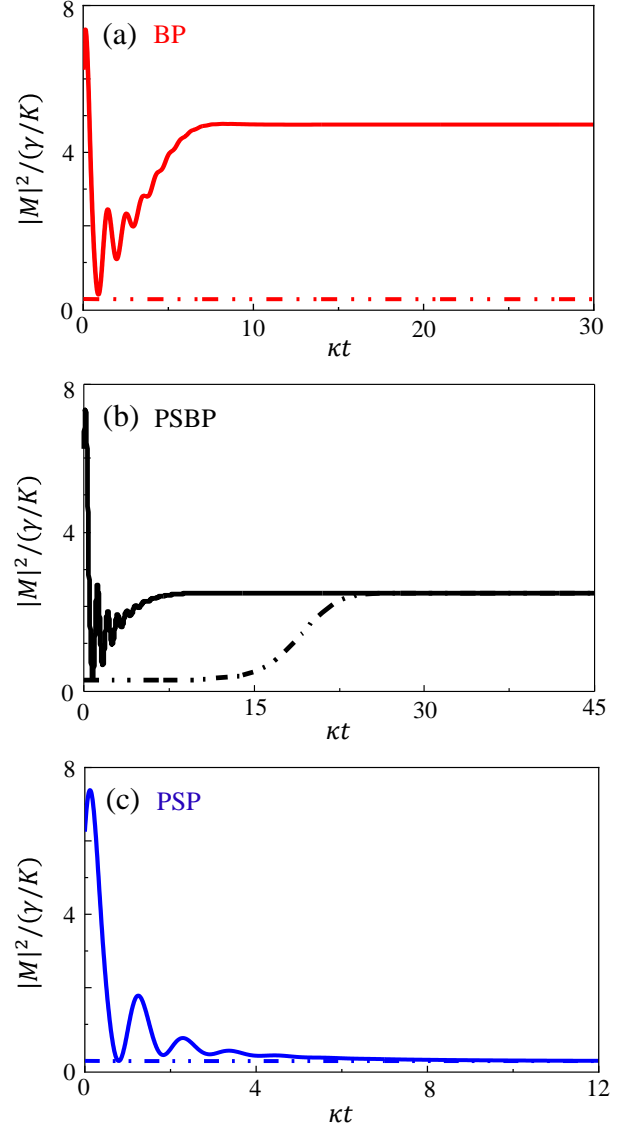


FIG. 3. Dynamics of the normalized magnon number for three phases at the points marked by different-colored dots in Fig. 2(b), with (a) $G/\kappa = 1.7$ and $\Delta_m/\Delta_c = 1$, (b) $G/\kappa = 2.3$ and $\Delta_m/\Delta_c = 1.2$, (c) $G/\kappa = 2.3$ and $\Delta_m/\Delta_c = 0.4$. In (a)-(c), $\langle a \rangle_{t=0} / \sqrt{\gamma/K} = 2 + 1.5i$ and $\langle b \rangle_{t=0} / \sqrt{\gamma/K} = 2 - 1.5i$ for the solid curves, while $\langle a \rangle_{t=0} / \sqrt{\gamma/K} = 0.05 + 0.05i$ and $\langle b \rangle_{t=0} / \sqrt{\gamma/K} = 0.05 - 0.05i$ for the dashed curves. The other parameters are $J/\kappa = 2.5$ and $\gamma/\kappa = 1$.

To exhibit the order of QPT and see its nonreciprocity more clearly, we focus on the behavior of the order parameter $|M|^2$ especially near the critical threshold for different Fizeau shifts Δ_F . In Fig. 4(a), the scaled steady-state magnon number $|M|^2 / (\gamma/K)$ is plotted as a function of the driving strength G/κ in the case of $\Delta_m/\Delta_c \geq \beta|_{G=G_{c1}}$. We find that the critical driving strength is $G = G_{c2}$ and $|M|^2 / (\gamma/K)$ changes continuously from zero, which means that the system undergoes a second-order phase transition from PSP to PSBP. When $G < G_{c2}$, the

system is in the PSP with $|M|^2 (\gamma/K) = 0$. However, in the case of $G > G_{c2}$, it is in the PSBP with $|M|^2 (\gamma/K) > 0$. Fig. 4(b) plots the scaled steady-state magnon number $|M|^2 / (\gamma/K)$ versus the driving strength G/κ for $\Delta_m/\tilde{\Delta}_a \leq \beta|_{G=G_{c1}}$. We see that $|M|^2 / (\gamma/K)$ has an obvious jumping behavior across the critical point G_{c1} , confirming a first-order phase transition from PSP to BP. Furthermore, it is found that different driving directions (the left or right) will lead to the QPT occurring at the different critical driving strength. In comparison with the stationary case with $\Delta_F = 0$, the critical driving strengths of phase transition of the spinning system always increases for $\Delta_F > 0$, while they decreases for $\Delta_F < 0$. Therefore, we can tune (increase or decrease) the critical driving strength effectively by adjusting the spinning direction and the spinning speed of the resonator. More specifically, we clearly see from Fig. 4 that the second- and one-order phase transitions respectively occur at $G/\kappa = 2.05, 1.97$ in the case of the stationary-resonator (i.e., $\Delta_F = 0$). By rotating the resonator, the position of the QPTs move towards the left (right) with $\Delta_F < 0$ ($\Delta_F > 0$), namely, the mean magnon numbers $|M|^2 / (\gamma/K)$ are respectively greater than zero from $G/\kappa > 1.84$ in Fig. 4(a) and $G/\kappa > 1.81$ in Fig. 4(b) when $\Delta_F/\kappa = -0.3$. $|M|^2 / (\gamma/K) > 0$ begin with $G/\kappa > 2.28$ in Fig. 4(a) and $G/\kappa > 2.16$ in Fig. 4(b) with $\Delta_F/\kappa = 0.3$. Moreover, to confirm the validity of the analytical calculation, we also numerically simulate the QPT behaviors of the system (the dashed curves), which are in high agreement with the analytical results (the solid curves). As a consequence, the magnon number $|M|^2 / (\gamma/K) > 0$ can be achieved for driving the resonator from one direction and $|M|^2 / (\gamma/K) = 0$ for driving from the opposite direction and thus the spinning-induced direction-dependent magnon number can be attributed to a nonreciprocal QPT.

Next, we reveal more characteristics of the nonreciprocal QPT through numerically observing the behavior of the correlated fluctuation of the magnon operators δm^\dagger and δm . As shown in Fig. 5, we plot the expectation value $\langle \delta m^\dagger \delta m \rangle$ of correlated fluctuation as a function of the scaled coupling strength G/κ for different values of Δ_F . There is a common characteristic in both Figures 5(a) and 5(b), that is, the mean correlated fluctuation $\langle \delta m^\dagger \delta m \rangle$ is close to zero when the driving strength G is away from the critical value, but Figure 5(a) (Figure 5(b)) is of an asymptotic (catastrophic) divergent behavior around the critical point, which is connected with the second-order QPT from PSP to PSBP (the first-order QPT from PSP to BP). From Fig. 5, we notice especially that spinning the resonator decreases the critical driving strength for $\Delta_F < 0$ or increases it for $\Delta_F > 0$, compared with the stationary-resonator case ($\Delta_F = 0$). Besides, associating Fig. 4 with Fig. 5 finds that the critical positions where the QPT occurs in Fig. 5(a) (Fig. 5(b)) completely agree with those in Fig. 4(a) (Fig. 4(b)) as we expected. The results give further evidence that the nonreciprocal QPT can be realized in the model.

Finally, to quantitatively describe the effect of spinning on

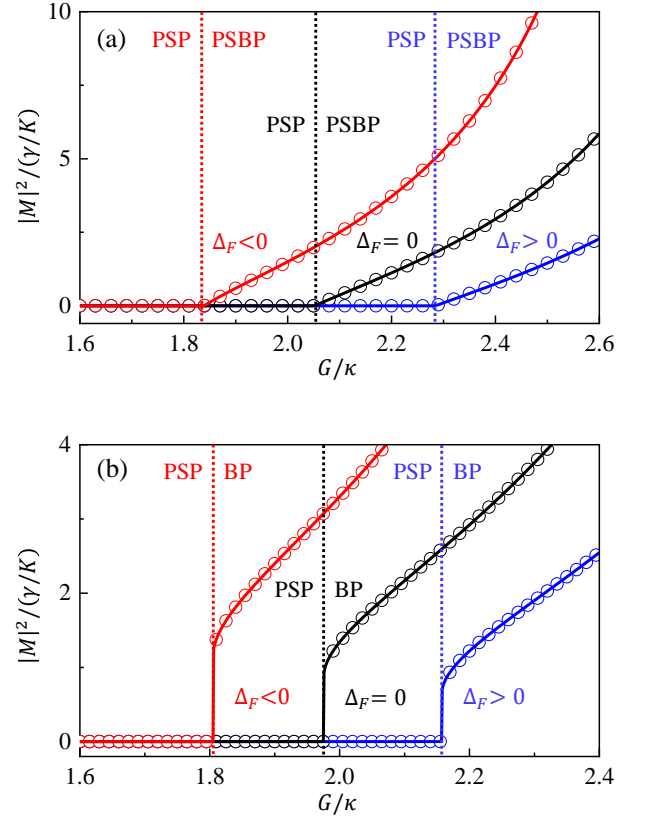


FIG. 4. Normalized steady-state magnon number $|M|^2 / (\gamma/K)$ is plotted as the scaled driving strength G/κ for three different Fizeau shifts $\Delta_F/\kappa = -0.3, 0$, and 0.3 . The solid curves correspond to the analytical results in Eq. (6) and the circles correspond to the numerical results obtained by Eq. (10). (a) $\Delta_m/\kappa = 4$ and initial conditions $\langle a \rangle_{t=0} / \sqrt{\gamma/K} = \langle b \rangle_{t=0} / \sqrt{\gamma/K} = 0.2 + 0.2i$, (b) $\Delta_m/\kappa = 2.2$ and initial conditions $\langle a \rangle_{t=0} / \sqrt{\gamma/K} = \langle b \rangle_{t=0} / \sqrt{\gamma/K} = 10 + 10i$. The other parameters are $\Delta_c/\kappa = 3$, $J/\kappa = 2.5$, and $\gamma/\kappa = 1$.

the nonreciprocal QPT, we introduce the isolation parameter

$$\mathfrak{R} = \begin{cases} 0, & |M|^2 (\Delta_F) = 0 \\ \frac{|M|^2 (\Delta_F < 0) - |M|^2 (\Delta_F > 0)}{|M|^2 (\Delta_F < 0) + |M|^2 (\Delta_F > 0)}, & \text{The other} \end{cases} \quad (13)$$

For a QPT without the spinning resonator (i.e., a conventional reciprocal QPT), the isolation parameter is $\mathfrak{R} = 0$. A nonzero \mathfrak{R} denotes the emergence of nonreciprocity in the phase transition. The higher the isolation parameter \mathfrak{R} is, the stronger the nonreciprocity of the QPT is. Especially, $\mathfrak{R} = 1$ corresponds to an ideal nonreciprocal QPT. The isolation parameter \mathfrak{R} as the function of the Fizeau shift $|\Delta_F|/\kappa$ is shown Figs. 6(a) and 6(b) for the second-order and first-order phase transitions, respectively. As expected, the isolation parameter is $\mathfrak{R} = 0$ for the QPT with a stationary resonator (i.e., $\Delta_F = 0$). While it is clear that, not only the nonreciprocal QPT occurs in a remarkably broad parameter range, but also the region of the ideal nonreciprocal QPT enlarges with the increasing of the Fizeau shift $|\Delta_F|$. Further, the ideal nonreciprocal QPT exists obviously two boundaries, one boundary condition (the left black curve) satisfies $G = G_{c2}$ ($\Delta_F < 0$) and the other one (the

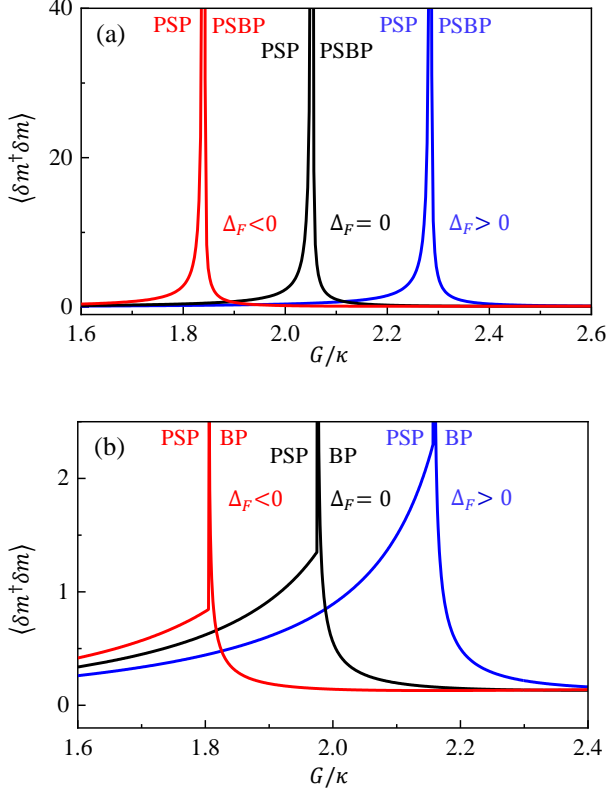


FIG. 5. Mean correlated fluctuation $\langle \delta m^\dagger \delta m \rangle$ as a function of the scaled driving strength G/κ for three different Fizeau shifts $\Delta_F/\kappa = -0.3, 0, \text{ and } 0.3$. The other parameters are the same with Figure 4.

right black curve) is $G = G_{c2}$ ($\Delta_F > 0$) in Fig. 5(a). In the same way, there exists a similar characteristic in Fig. 5(b). An interesting feature in Fig. 6 is that in the vicinity of the left black curves, the isolation parameter \mathfrak{R} experiences a sudden change from zero to one. That is because both mean magnon numbers $|M|^2$ ($\Delta_F < 0$) and $|M|^2$ ($\Delta_F > 0$) are zero when the driving strength is less than the critical strength. However, when the driving strength is more than the critical strength, $|M|^2$ ($\Delta_F < 0$) is nonzero and $|M|^2$ ($\Delta_F > 0$) is still zero. In this situation, we see that the isolation parameter \mathfrak{R} undergoes a gradually change from one to zero. It can be well understood that $|M|^2$ ($\Delta_F < 0$) is nonzero and $|M|^2$ ($\Delta_F > 0$) is zero when the driving strength is less than the critical strength, on the other hand, when the driving strength is more than the critical strength, both $|M|^2$ ($\Delta_F < 0$) and $|M|^2$ ($\Delta_F > 0$) are not only nonzero, but also gradually increasing with the driving strength increasing.

IV. CONCLUSIONS

In summary, we have theoretically studied the role of rotation in engineering an nonreciprocal quantum phase transition

in the cavity magnonic system consisting of a YIG sphere coupled to a spinning microwave resonator. By rotating the microwave resonator, we show that the introduced Sagnac effect

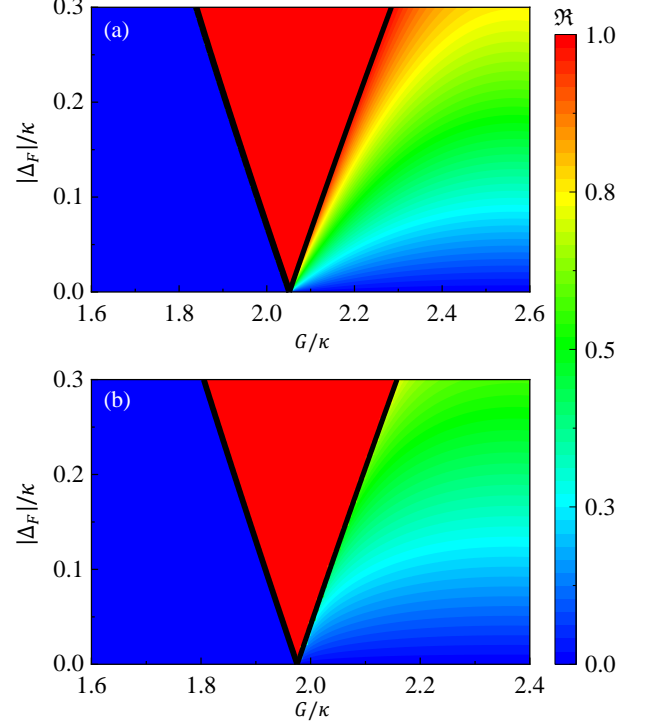


FIG. 6. Isolation parameter \mathfrak{R} versus the scaled Fizeau shift $|\Delta_F|/\kappa$ and normalized driving strength G/κ . The left and right black curves correspond to the boundary conditions in Eqs. (8) and (9), respectively. The parameters are the same as those in Figure 2.

can significantly modify the critical driving strengths for both second- and first-order quantum phase transitions and lead to a largely adjustable range of the critical driving strength. We further find that the critical driving strength of the phase transition relies on both the driving direction (or the rotation direction) and the spinning speed. In consequence, a highly tunable nonreciprocal quantum phase transition can be achieved based on the Sagnac effect. Our proposal provides an alternative route to achieve nonreciprocal quantum phase in microwave magnonic system and may find promising applications in designing nonreciprocal magnonic devices.

ACKNOWLEDGMENTS

This work is supported by the National Science Foundation for Distinguished Young Scholars of the Higher Education Institutions of Anhui Province (Grant No. 2022AH020097). G. Q. Zhang is supported by the National Natural Science Foundation of China (Grant No. 12205069).

Note added. -In preparing our manuscript, we became aware of a similar work on nonreciprocal superradiant phase transitions published on Physical Review Letters [67].

-
- [1] S. S. Sachdev, *Quantum Phase Transitions*, 2nd ed. (Cambridge University Press, Cambridge, 2011).
- [2] L. Sondhi, S. M. Girvin, J. P. Carini, and D. Shahar, Continuous quantum phase transitions, *Rev. Mod. Phys.* 69(1), 315 (1997).
- [3] C. Emary and T. Brandes, Chaos and the quantum phase transition in the Dicke model, *Phys. Rev. E* 67, 066203 (2003).
- [4] F. Dimer, B. Estienne, A. S. Parkins, and H. J. Carmichael, Proposed realization of the Dicke-model quantum phase transition in an optical cavity QED system, *Phys. Rev. A* 75, 013804 (2007).
- [5] K. Baumann, R. Mottl, F. Brennecke, and T. Esslinger, Exploring symmetry breaking at the Dicke quantum phase transition, *Phys. Rev. Lett.* 107, 140402 (2011).
- [6] T. L. Wang, L. N. Wu, W. Yang, G. R. Jin, N. Lambert, and F. Nori, Quantum Fisher information as a signature of the superradiant quantum phase transition, *New J. Phys.* 16(6), 063039 (2014).
- [7] H. T. Mebrahtu, I. V. Borzenets, D. E. Liu, H. Zheng, Y. V. Bomze, A. I. Smirnov, H. U. Baranger, and G. Finkelstein, Quantum phase transition in a resonant level coupled to interacting leads, *Nature (London)* 488, 61 (2012).
- [8] J. Zhang, C. Z. Chang, P. Tang, Z. Zhang, X. Feng, K. Li, L. Wang, X. Chen, C. Liu, W. Duan, K. He, Q. K. Xue, X. Ma, and Y. Wang, Topology-driven magnetic quantum phase transition in topological insulators, *Science* 339, 1582 (2013).
- [9] M. J. Hwang, R. Puebla, and M. B. Plenio, Quantum Phase Transition and Universal Dynamics in the Rabi Model, *Phys. Rev. Lett.* 115, 180404 (2015).
- [10] X. Y. Lü, L. L. Zheng, G. L. Zhu, and Y. Wu, Single-Photon-Triggered Quantum Phase Transition, *Phys. Rev. Appl.* 9, 064006 (2018).
- [11] G. Q. Zhang, Z. Chen, and J. Q. You, Experimentally accessible quantum phase transition in a non-Hermitian Tavis-Cummings model engineered with two drive fields, *Phys. Rev. A* 102, 032202 (2020).
- [12] X. Chen, Z. Wu, M. Jiang, X. Y. Lü, X. Peng, and J. Du, Experimental quantum simulation of superradiant phase transition beyond no-go theorem via antisqueezing, *Nat. Commun.* 12, 6281 (2021).
- [13] J. F. Huang and L. Tian, Modulation-based superradiant phase transition in the strong-coupling regime, *Phys. Rev. A* 107, 063713 (2023).
- [14] W. Huang, Y. Wu, and X. Y. Lü, Superradiant phase transition induced by the indirect Rabi interaction, *Phys. Rev. A* 107, 033702 (2023).
- [15] B. Wang, F. Nori, and Z. L. Xiang, Quantum phase transitions in optomechanical systems, *Phys. Rev. Lett.* 132, 053601 (2024).
- [16] C. Liu and J. F. Huang, Quantum phase transition of the Jaynes-Cummings model, *Sci. China Phys. Mech. Astron.* 67, 210311 (2024).
- [17] M.-J. Hwang, R. Puebla, and M. B. Plenio, Quantum phase transition and universal dynamics in the Rabi model, *Phys. Rev. Lett.* 115, 180404 (2015).
- [18] Y. F. Xie, X. Y. Chen, X. F. Dong, and Q. H. Chen, First-order and continuous quantum phase transitions in the anisotropic quantum Rabi-Stark model, *Phys. Rev. A* 101, 053803 (2020).
- [19] M. L. Cai, Z. D. Liu, W. D. Zhao, Y. K. Wu, Q. X. Mei, Y. Jiang, L. He, X. Zhang, Z. C. Zhou, and L. M. Duan, Observation of a quantum phase transition in the quantum Rabi model with a single trapped ion, *Nat. Commun.* 12, 1126 (2021).
- [20] C. J. Zhu, L. L. Ping, Y. P. Yang, and G. S. Agarwal, Squeezed light induced symmetry breaking superradiant phase transition, *Phys. Rev. Lett.* 124, 073602 (2020).
- [21] X. H. H. Zhang and H. U. Baranger, Driven-dissipative phase transition in a Kerr oscillator: From semiclassical PT symmetry to quantum fluctuations, *Phys. Rev. A* 103, 033711 (2021).
- [22] G. Liu, W. Xiong, and Z. J. Ying, Switchable superradiant phase transition with Kerr magnons, *Phys. Rev. A* 108, 033704 (2023).
- [23] G. Q. Zhang, Z. Chen, W. Xiong, C. H. Lam, and J. Q. You, Parity-symmetry-breaking quantum phase transition via parametric drive in a cavity magnonic system, *Phys. Rev. B* 104, 064423 (2021).
- [24] Y. Qin, S. C. Li, K. Li, and J. J. Song, Controllable quantum phase transition in a double-cavity magnonic system, *Phys. Rev. B* 106, 054419 (2022).
- [25] D. Jalas, A. Petrov, M. Eich, W. Freude, S. Fan, Z. Yu, R. Baets, M. Popović, A. Melloni, J. D. Joannopoulos, M. Vanwolleghem, C. R. Doerr, and H. Renner, What is- and what is not - an optical isolator, *Nat. Photon.* 7, 579 (2013).
- [26] D. L. Sounas and A. Alù, Non-reciprocal photonics based on time modulation, *Nat. Photonics* 11, 774 (2017).
- [27] A. A. Mazneva, A. G. Every, and O. B. Wright, Reciprocity in reflection and transmission: What is a ‘phonon diode’?, *Wave Motion* 50, 776 (2013).
- [28] R. Fleury, D. L. Sounas, C. F. Sieck, M. R. Haberman, and A. Alù, Sound Isolation and Giant Linear Nonreciprocity in a Compact Acoustic Circulator, *Science* 343, 516 (2014).
- [29] B. I. Popa and S. A. Cummer, Non-reciprocal and highly nonlinear active acoustic metamaterials, *Nat. Commun.* 5, 3398 (2014).
- [30] D. Torrent, O. Poncelet, and J. C. Batsale, Nonreciprocal Thermal Material by Spatiotemporal Modulation, *Phys. Rev. Lett.* 120, 125501 (2018).
- [31] J. D. Adam, L. E. Davis, G. F. Dionne, E. F. Schloemann, and S. N. Stitzer, Ferrite devices and materials, *IEEE Trans. Microw. Theory Technol.* 50, 721 (2002).
- [32] H. Dötsch, N. Bahlmann, O. Zhuromskyy, M. Hammer, L. Wilkens, R. Gerhardt, P. Hertel, and A. F. Popkov, Applications of magneto-optical waveguides in integrated optics: review, *J. Opt. Soc. Am. B* 22, 240 (2005).
- [33] L. Fan, J. Wang, L. T. Varghese, H. Shen, B. Niu, Y. Xuan, A. M. Weiner, and M. Qi, An all-silicon passive optical diode, *Science* 335, 447 (2012).
- [34] Q. T. Cao, H. Wang, C. H. Dong, H. Jing, R. S. Liu, X. Chen, L. Ge, Q. Gong, and Y. F. Xiao, Experimental demonstration of spontaneous chirality in a nonlinear microresonator, *Phys. Rev. Lett.* 118, 033901 (2017).
- [35] A. R. Hamann, C. Müller, M. Jerger, M. Zanner, J. Combes, M. Pletyukhov, M. Weides, T. M. Stace, and A. Fedorov, Nonreciprocity Realized with Quantum Nonlinearity, *Phys. Rev. Lett.* 121, 123601 (2018).
- [36] X. W. Xu, Y. Li, B. Li, H. Jing, and A. X. Chen, Nonreciprocity via Nonlinearity and Synthetic Magnetism, *Phys. Rev. Applied* 13, 044070 (2020).
- [37] S. Manipatruni, J. T. Robinson, and M. Lipson, Optical Nonreciprocity in Optomechanical Structures, *Phys. Rev. Lett.* 102, 213903 (2009).
- [38] Z. Shen, Y.-L. Zhang, Y. Chen, C.-L. Zou, Y.-F. Xiao, X.-B. Zou, F.-W. Sun, G.-C. Guo, and C.-H. Dong, Experimental realization of optomechanically induced non-reciprocity, *Nat. Photonics* 10, 657 (2016).

- [39] N. R. Bernier, L. D. Tóth, A. Koottandavida, M. A. Ioannou, D. Malz, A. Nunnenkamp, A. K. Feofanov, and T. J. Kippenberg, Nonreciprocal reconfigurable microwave optomechanical circuit, *Nat. Commun.* 8, 604 (2017).
- [40] H. Ramezani, T. Kottos, R. El-Ganainy, and D. N. Christodoulides, Unidirectional nonlinear PT-symmetric optical structures, *Phys. Rev. A* 82, 043803 (2010).
- [41] B. Peng, S. K. Özdemir, F. Lei, F. Moni, M. Gianfreda, G. L. Long, S. Fan, F. Nori, C. M. Bender, and L. Yang, Parity-time-symmetric whispering-gallery microcavities, *Nature Phys.* 10, 394 (2014).
- [42] L. Chang, X. Jiang, S. Hua, C. Yang, J. Wen, L. Jiang, G. Li, G. Wang, and M. Xiao, Parity-time symmetry and variable optical isolation in active-passive-coupled microresonators, *Nature Photon.* 8, 524 (2014).
- [43] X. Huang, C. Lu, C. Liang, H. Tao, and Y.-C. Liu, Loss-induced nonreciprocity, *Light Sci. Appl.* 10, 30 (2021).
- [44] S. Maayani, R. Dahan, Y. Kligerman, E. Moses, A. U. Hassan, H. Jing, F. Nori, D. N. Christodoulides, and T. Carmon, Flying couplers above spinning resonators generate irreversible refraction, *Nature (London)* 558, 569 (2018).
- [45] R. Huang, A. Miranowicz, J.-Q. Liao, F. Nori, and H. Jing, Nonreciprocal photon blockade, *Phys. Rev. Lett.* 121, 153601 (2018).
- [46] K. Wang, Q. Wu, Y. F. Yu, and Z. M. Zhang, Nonreciprocal photon blockade in a two-mode cavity with a second-order nonlinearity, *Phys. Rev. A* 100, 053832 (2019).
- [47] B. Li, R. Huang, X. Xu, A. Miranowicz, and H. Jing, Nonreciprocal unconventional photon blockade in a spinning optomechanical system, *Photon. Res.* 7, 630 (2019).
- [48] H. Z. Shen, Q. Wang, J. Wang, and X. X. Yi, Nonreciprocal unconventional photon blockade in a driven dissipative cavity with parametric amplification, *Phys. Rev. A* 101, 013826 (2020).
- [49] Y. W. Jing, H. Q. Shi, and X. W. Xu, Nonreciprocal photon blockade and directional amplification in a spinning resonator coupled to a two-level atom, *Phys. Rev. A* 104, 033707 (2021).
- [50] W. Zhang, T. Wang, S. Liu, S. Zhang, and H.-F. Wang, Nonreciprocal photon blockade in a spinning resonator coupled to two two-level atoms, *Sci. China Phys.* 66, 240313 (2023).
- [51] X. Y. Yao, H. Ali, F. L. Li, and P. B. Li, Nonreciprocal phonon blockade in a spinning acoustic ring cavity coupled to a two-level system, *Phys. Rev. Applied* 17, 054004 (2022).
- [52] N. Yuan, S. He, S. Y. Li, N. Wang, and A. D. Zhu, Optical noise-resistant nonreciprocal phonon blockade in a spinning optomechanical resonator, *Opt. Express* 31, 20160 (2023).
- [53] Y. Wang, W. Xiong, Z. Xu, G. Q. Zhang, and J. Q. You, Dissipation-induced nonreciprocal magnon blockade in a magnon-based hybrid system, *Sci. China Phys. Mech. Astron.* 65, 260314 (2022).
- [54] K. W. Huang, X. Wang, Q. Y. Qiu, and H. Xiong, Nonreciprocal magnon blockade via the Barnett effect, *Opt. Lett.* 49, 758 (2024).
- [55] Y. F. Jiao, S. D. Zhang, Y. L. Zhang, A. Miranowicz, L. M. Kuang, and H. Jing, Nonreciprocal Optomechanical Entanglement against Backscattering Losses, *Phys. Rev. Lett.* 125, 143605 (2020).
- [56] W. Zhong, Q. Zheng, G. Cheng, and A. Chen, Nonreciprocal genuine steering of three macroscopic samples in a spinning microwave magnon system, *Appl. Phys. Lett.* 123, 134003 (2023).
- [57] S. Chakraborty and C. Das, Nonreciprocal magnon-phonon entanglement in cavity magnomechanics, *Phys. Rev. A* 108, 063704 (2023).
- [58] J. Chen, X. G. Fan, W. Xiong, and L. Ye, Nonreciprocal photon-phonon entanglement in Kerr-modified spinning cavity magnomechanics, *Phys. Rev. A* 109, 043512 (2024).
- [59] S. S. Chen, S. S. Meng, H. Deng, and G. J. Yang, Nonreciprocal mechanical squeezing in a spinning optomechanical system, *Ann. Phys.* 533, 2000343 (2021).
- [60] Q. Guo, K. X. Zhou, C. H. Bai, Y. Zhang, G. Li, and T. Zhang, Nonreciprocal mechanical squeezing in a spinning cavity optomechanical system via pump modulation, *Phys. Rev. A* 108, 033515 (2023).
- [61] B. Zhao, K. X. Zhou, M. R. Wei, J. Cao, and Q. Guo, Nonreciprocal strong mechanical squeezing based on the Sagnac effect and two-tone driving, *Opt. Lett.* 49, 486 (2024).
- [62] Y. Jiang, S. Maayani, T. Carmon, F. Nori, and H. Jing, Nonreciprocal Phonon Laser, *Phys. Rev. Applied* 10, 064037 (2018).
- [63] Y. Xu, J. Y. Liu, W. Liu, and Y. F. Xiao, Nonreciprocal phonon laser in a spinning microwave magnomechanical system, *Phys. Rev. A* 103, 053501 (2021).
- [64] Y. J. Xu and J. Song, Nonreciprocal magnon laser, *Opt. Lett.* 46, 5276 (2021).
- [65] W. A. Li, G. Y. Huang, J. P. Chen, and Y. Chen, Nonreciprocal enhancement of optomechanical second-order sidebands in a spinning resonator, *Phys. Rev. A* 102, 033526 (2020).
- [66] X. Wang, K. W. Huang, and H. Xiong, Nonreciprocal sideband responses in a spinning microwave magnomechanical system, *Opt. Express* 31, 5492 (2023).
- [67] G. L. Zhu, C. S. Hu, H. Wang, W. Qin, X. Y. Lü, and F. Nori, Nonreciprocal superradiant phase transitions and multicriticality in a cavity QED system, *Phys. Rev. Lett.* 132, 293602 (2024).